ORIGINAL ARTICLE

Compression and low velocity impact response of wood-based sandwich panels with auxetic lattice core

Jerzy Smardzewski[1] · Michał Maslej[1] · Krzysztof W. Wojciechowski[2,3]

Abstract

The research determined the resistance to compression and low velocity impact of wood-based sandwich panels, the face sheet made of high-density fiber board, and high pressure laminate, while its auxetic lattice core was made by 3D printing using LayWood bio-composite filament. The core's auxetic property (i.e. exhibiting negative Poisson's ratio) was observed within the planes parallel to the facings. The ability of particular types of multilayer panels to absorb the energy was also determined. Based on the analysis of the obtained test results, it was proven that the core denoted as B, with inclination angle of the cell ribs $\varphi_x = \varphi_y = 65°$, shows the highest compressive strength. It was determined that the dynamic load causes a very high overload in high-density fiber board face sheets. This results in damage to the sandwich panel surface and core structure. Cells of type B favorably minimize the differences in absorbed energy when using different face sheets and the energy value for low velocity impact. Taking into account the amount of absorbed energy, the most attractive is the panel with the D-type orthotropic core characterized by an inclination angle of the cell ribs $\varphi_x = 30°$, $\varphi_y = 60°$. The amount of energy absorbed by samples with high-density fiberboard face sheets increases significantly depending on the impactor's energy. For panels with face sheets manufactured from high-pressure laminate, the amount of energy absorbed decreases.

1 Introduction

Multilayer lightweight panels consist of outer cover face sheets and a core. Face sheets can be made of rigid and strong materials resistant to static or dynamic normal forces, bending, or torsional moments. Cores of multilayer structures are usually made of lightweight and elastic materials resistant to tangential forces. Sandwich panels used in construction or thin-walled structures can behave like ductile materials under static load. On the other hand, they can behave like brittle material under impact and be more susceptible to damages, such as punctures, crushing, breakage of face sheet surfaces. These properties are particularly desirable for materials used in aviation, automotive, buildings, and furniture industry. Therefore, the quality of the lightweight panels can be assessed by impact resistance criteria. The influence of low velocity impacts on the strength, deflection and amount of absorbed energy of honeycomb sandwich panels with hexagonal core, made of metal and artificial composites was studied experimentally, analytically and numerically (Chen et al. 2017; Guj and Sestieri 2007; Menna et al. 2013; Schwingshackl et al. 2006; Sun et al. 2018; Xue and Hutchinson 2006).

In terms of the stiffness and strength of honeycomb panels, sandwich panels with the following types of core are much stronger: coating (Kavermann and Bhattacharyya 2019; Smardzewski and Jasińska 2016), lattice truss (Jin et al. 2015; Xu et al. 2016), pyramidal (Qi and Ma 2018; Xiong et al. 2014a, b; Xu et al. 2015), kagome (Klimek et al. 2016) cubic or cubic + octet (isomax) (Yazdani Sarvestani et al. 2018). Wang (2019) made a comprehensive overview on the development of the innovative honeycomb-based structures in the past two decades. The author suggested that innovative honeycomb will still be a hotspot in the field of impact resistance, packing, blast protection, and other engineering applications in the future.

In addition to the above-listed mechanical properties, the ability of these panels to absorb energy during low velocity

✉ Jerzy Smardzewski
  jsmardzewski@up.poznan.pl

[1] Faculty of Wood Technology, Department of Furniture Design, Poznan University of Life Sciences, Wojska Polskiego 28, Poznan, Poland

[2] Institute of Molecular Physics Polish Academy of Sciences, M. Smoluchowskiego 17, 60-179 Poznań, Poland

[3] Akademia Kaliska im. Prezydenta Stanisława Wojciechowskiego, ul. Nowy Świat 4, 62-800 Kalisz, Poland

impact was also studied. Mines et al. (2013) found that under such a load, the mechanical properties of aluminum sandwich panels with a micro-pyramidal core are similar to those of an aluminum honeycomb panel with a hexagonal core. He et al. (2018) determined the low-velocity impact resistance of hybrid sandwich panels with face sheets made of carbon fiber-reinforced polymer (CFRP) and trapezoidal aluminum core. Studies by Yazdani Sarvestani et al. (2018) have proven that metasandwich isomax structures have a high quasi-static and dynamic ability to absorb impact energy. Kao et al. (2018) determined the impact strength of a lattice beam filled with foam made of biocomposites (polylactide PLA). The foam has a positive effect on the structure's mechanical properties by increasing the system's absorption energy. Han et al. (2017) studied ultra-thin panels with prismatic, hexagonal, coating, and pyramidal cores made of metal. The core's free spaces were filled with ceramic materials, concrete, and polymer or metal foam. The panels with filling are characterized by high resistance and the ability to absorb impact energy. In the case of foamless systems (Gao et al. 2019), the impact strength of a double-arrow auxetic (i.e. exhibiting negative Poisson's ratio) pyramidal structure is more sensitive to the geometric parameters of a longer arm than of a short arm. Boonkong et al. (2016) performed numerical calculations simulating a low velocity impact on the surfaces of an aluminum panel with a corrugated core.

There has been little research in this area concerning multilayer lightweight panels made of materials of plant origin. Contemporary interest in biodegradable materials and attempts to apply them in practice are aimed to reduce the burden on the environment, with stiffness and strength of sandwich panels similar to conventional materials. The use of natural resources can reduce carbon dioxide emissions and the greenhouse effect (Bogoeva-Gaceva et al. 2007; Holbery and Houston 2006; Mohanty et al. 2002). The popular wood-based honeycomb panels available on the market consist of a paper core with hexagonal cells covered with high or medium density fiber boards (HDF, MDF), plywood (PW), or particle board (PB). The total thickness of boards with 3 mm thick HDF, MDF, or PW face sheets is between 18 and 25 mm. Among the 38 mm, 50 mm, and 60 mm thick boards, particle board face sheets with a thickness of 8 mm dominate. Due to lower stiffness and strength compared to P2 type furniture particle boards, honeycomb panels with a thickness of up to 25 mm are not used to design elements under bending or twisting loads (Barboutis and Vassiliou 2005; Smardzewski et al. 2018). Thick honeycomb panels are popular in buildings as insulating materials (Klimek et al. 2016; Sam-Brew et al. 2011). Given the buildings and furniture industries' needs, it is expedient to replace traditional honeycomb boards with thin sandwich panels with a lattice core.

In the paper by Mohammadabadi et al. (2018), the authors described the low velocity impact response of wood-based sandwich panels with a corrugated core made of oriented strand board (OSB). The effect of the contact area between the impactor and the sample was investigated using impact loads with cylindrical and semicircular impactors. The effect of filling the core cavities with foam insulation material was studied to understand the changes in energy absorption and differences in the samples' modes of damage. The observed damage modes for all sandwich panels with and without foam, tested using both these types of impacts, were splitting, perforation, penetration, crushing, and tearing occurring between the core and the outer layers. Panels with core voids filled with foam absorbed 26% more energy than unfilled panels.

Based on the above mentioned literature review and to the best of the authors` knowledge, no studies have been carried out so far on the low velocity impact response of wood-based sandwich panels with auxetic lattice cores. In a few cases, only metal panels with auxetic hexagonal (Jin et al. 2016) or chiral cores (Spadoni et al. 2005) were examined. To further improve lightweight wood-based sandwich panels' response to low velocity impacts, the complex and auxetic multilayer structure can be used. Auxetic materials (structures) improve the mechanical properties of panels, especially shear resistance, bending resistance, impact resistance, and increase the ability to absorb energy (Li and Wang 2017; Zhang et al. 2015). Models of structures with a negative Poisson's ratio have been described more than 30 years ago (Almgren 1985; Kolpakov 1985; Wojciechowski 1987, 1989). The first real material (foam) of such a property was manufactured by Lakes in 1987 (Lakes 1987). Materials of negative Poisson's ratio were coined auxetics by Evans (1991). Since then, many scientific papers and reviews presenting the properties and advantages of auxetics in relation to ordinary (positive Poisson's ratio) materials have been published. It should be mentioned the work edited by Wojciechowski et al. (2020), reviews by Lakes (2017), Lim (2017), Yu et al. (2018) as well as the book by Lim (2015), where references to various review articles, thematic issues and original publications on auxetic and corresponding systems can be found. The works mentioned above made it possible to design and manufacture, from materials of biological origin, pyramidal cores with auxetic properties (Maslej and Smardzewski 2019). In this study, the effect of the type of filament used in 3D printing and the geometry of pyramidal core cells on elastic constants in cores with identical relative density was determined. In the paper by Smardzewski and Wojciechowski (2019) an investigation based on the design of a thin sandwich panel with auxetic lattice core using wood composites and 3D print technology was initiated. The effect of variations in auxetic lattice core geometry and relative density on the mechanical properties of a wood-based composite was evaluated. The results provided by the bending test showed that mechanical properties

increase with increasing inclination angle of struts and relative density of the core.

Given the above, research was undertaken to determine the resistance to compression and low velocity impact of wood-based sandwich panels, the face sheet of which was made of high density fiber board (HDF) and high pressure laminate (HPL), while the auxetic lattice core was made of LayWood biocomposite. It was also decided to determine the ability of particular types of honeycomb panels to absorb the energy.

2 Materials and methods

2.1 Samples

According to previous tests, the cores with a height of $t_c = 10$ mm were made in 3D printing technology from LayWood's filament (LW) (Smardzewski et al. 2018). The general geometry of the core cells and dimensions is shown in Fig. 1 and Table 1. Sandwich panel face sheets are manufactured of wood: high density fiber board (HDF) with a nominal thickness of 2.95 mm, and high pressure laminate (HPL) with a thickness of 1.2 mm. HPL consisted of a protective layer made of specially impregnated paper with corundum, a
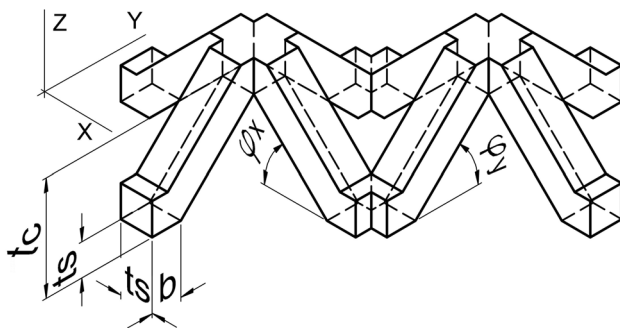
decorative layer made of paper impregnated with melamine resin, and a core paper of the highest hardness level impregnated phenolic resin (Swiss Krono Sp. z o.o., Żary, Poland). The layers of the core paper were arranged perpendicular to each other. Before bonding, lattice cores' extreme horizontal surfaces were degreased with technical acetone (Klingon, OGB Sp. z o.o., Poland). Then, the face sheets' wide internal surfaces were covered with a waterborne PVAc Pattex type adhesive (Henkel Polska Sp. z o.o., Warsaw, Poland) with a viscosity of 8000—15,000 mPas. The adhesive was applied to face sheet surfaces in the amount of 120 g/m². The samples of panels were prepared in such a way that the cores were placed between the face sheets with the adhesive-coated surfaces facing the center of the set. Then, a uniform pressure of 3.472 kPa was exerted on the set for 24 h. The gluing was carried out in laboratory conditions at relative humidity of 65% and temperature of 21 °C. After this time, the samples were seasoned in the same laboratory for the next two weeks to ensure hygroscopic balance with the ambient air. In Fig. 2 and Table 1, the dimensions of individual sample types A, B, C, D, E are presented. In laboratory studies, 5 replicates were used for each test, 200 samples in total. Figure 3 illustrates the samples prepared for the test.

2.2 Physico-mechanical properties of materials and cores

To correctly interpret the experimental results, it was decided to determine the materials' physico-mechanical properties by the uniaxial tensile test. The shape and dimensions of the samples are shown in Fig. 4 and Table 2. Due to the mutually perpendicular orientation of the paper fibers in the HPL core layer, samples with longitudinal (Y) and transverse (X) fiber layout in relation to the stretching direction were prepared for experimental tests. The samples were subjected to uniaxial tension on a universal testing machine ZWICK 1445 (Zwick Roell GmbH & Co.KG, Ulm, Germany) with a measuring range of 10 kN, an accuracy of force

Fig. 1 Shape and dimensions of the core cells

Table 1 Dimensions of samples and lattice cores

Core type	Dimension of core cells					Dimension of samples					
						HPL	HDF	Compression tests		Impact tests	
	t_c	t_s	b	φ_x	φ_y	t		m	n	m	n
	mm			°		mm					
A	10.8	3.0	2.7	45	45	13.2	16.7	58	58	120	120
B	11.0	2.0	2.3	65	65	13.4	16.9				
C	10.2	4.0	2.9	26	26	12.6	16.1				
D	10.8	3.0	3.2	30	60	13.2	16.7				
E	10.3	3.0	2.3	60	30	12.7	16.2				

Fig. 2 Shape and dimensions of samples A, B, C, D, E, intended for: **a** uniaxial compression, **b** low velocity impact
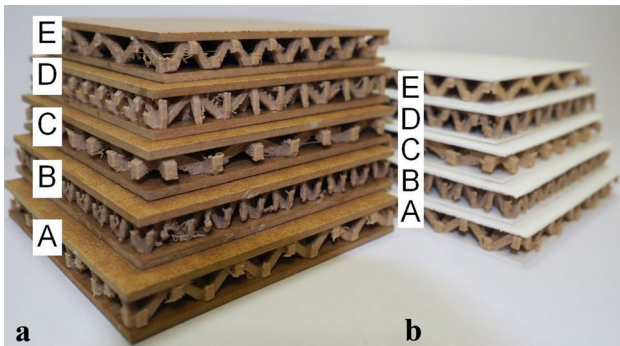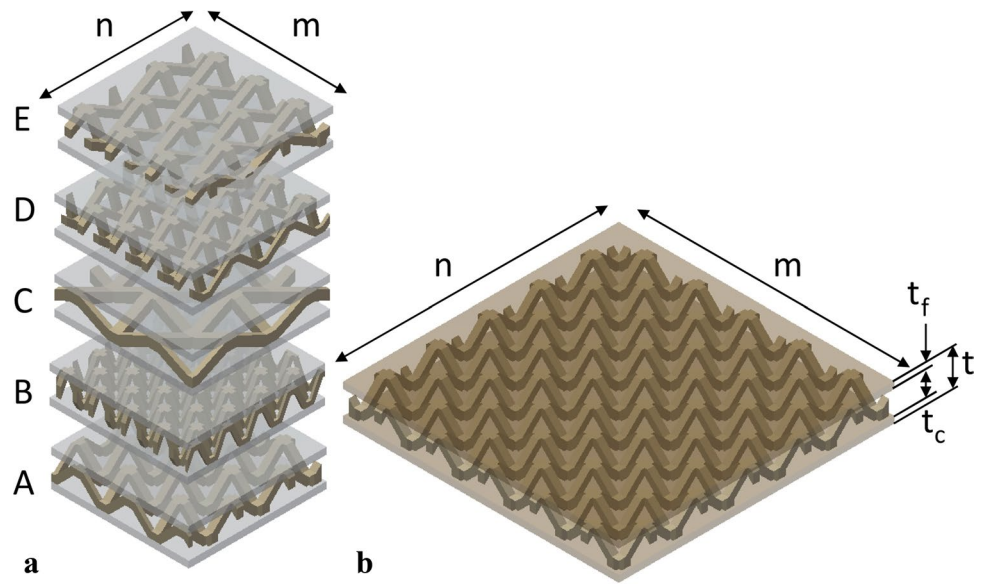
Fig. 3 Samples used for testing, face sheets: **a** HDF, **b** HPL

measurement of 0.01 N, displacement accuracy of 0.01 mm, and rate of placing loads of 2 mm/min. Elongations and shortenings in the middle part of the samples subjected to tension were recorded by digital image correlation and tracking (DICT) using Dantec Dynamics A/S (Skovlunde, Denmark). The accuracy of the measurement was 0.001 mm. For each type of material and test, 10 samples were used, 40 in total. Poisson's v_{yx}, v_{xy}, and linear elastic modulus E_x, E_y (MPa) were calculated based on converting the values of the measured deformations for the X and Y directions, respectively. The tensile strength σ_x, σ_y (MPa), material density and absolute moisture content MC (%) were also determined (Table 3). Table 3 shows that HPL is characterized by the highest density, followed by LW and HDF, with a value of 986 kg/m³, 903 kg/m³, and 852 kg/m³, respectively. These materials differ significantly also in terms of linear elasticity modulus. HPL has the highest value of the modulus E_y = 11.197 MPa. Linear elastic modulus of HPL for X direction and elastic modulus of HDF and LW are lower by 13.2%, 64.6%, and 92.5%, respectively, while tensile strength is
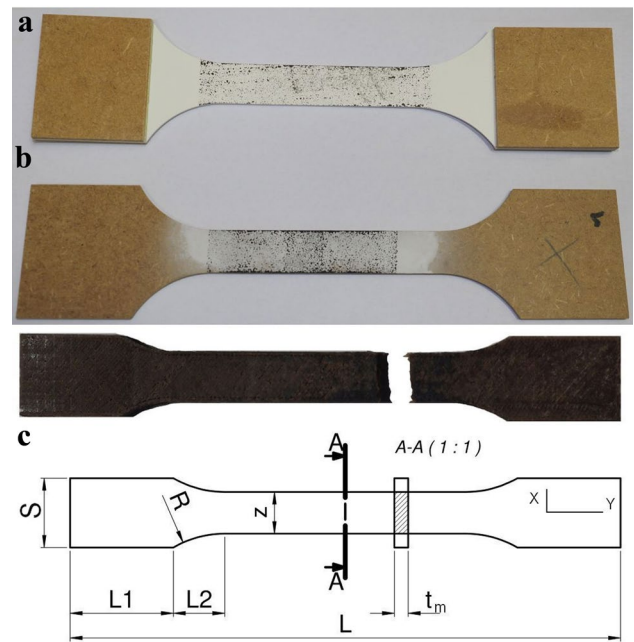
Fig. 4 Shape and dimensions of samples for determination of mechanical properties in axial tensile test: **a** HPL, **b** HDF, **c** LayWood

lower by 30.1%, 64.1%, and 82.9%, respectively, compared to the reference sample of HPL. The presented differences in mechanical properties will significantly influence the impact resistance of the sandwich panels tested. It is also expected that this resistance will depend on the elastic properties of the core. These properties, especially the modulus of linear elasticity E_{cy}, E_{cx} and Poisson's ratio, are described in detail in the paper by Smardzewski et al. (2018). This paper shows that the A, B, C cores exhibit isotropic properties, with C type core showing the most favorable elastic

Table 2 Dimensions of samples for determination of mechanical properties in axial tensile test

Properties	Unit	Material		
		HPL	HDF	LW
L	mm	250		160
L_1		50		30
L_2		30		15
S		60		
		20		20
z		30		12
R				30
t_m		1.20	2.95	4

Fig. 5 Sample of a sandwich panel during uniaxial compression

constants ($E_{cy} = E_{cx} = 15.36 MPa$, $\vartheta_{xy} = \vartheta_{yx} = -0.5197$). Orthotropic properties characterize D and E cores, but E type core has the highest elastic constants ($E_{cy} = 28.35 MPa$, $E_{cx} = 3.75 MPa$, $\vartheta_{xy} = -0.1163$, $\vartheta_{yx} = -1.3113$). Therefore, an increase in resistance to compression and impact could be expected among panels with cores with higher mechanical properties.

2.3 Experiments

2.3.1 Uniaxial compression

Uniaxial compression tests (Fig. 5) were made on a universal testing machine ZWICK 1445 (ZwickRoell GmbH & Co.KG, Ulm, Germany) with a measuring range of 10 kN, load measurement accuracy of 0.01 N, displacement accuracy of 0.01 mm, and load exertion velocity of 2 mm/min. During compression, the force and displacement were recorded until a load drop of 100 N compared to the maximum value was achieved. On this basis, the relationship between load and deflection for each type of core was developed.

2.3.2 Low velocity impact

Many publications describe commercial devices for testing energy absorbed during impact (Kiliçaslan et al. 2013; Liu et al. 2017; Yazdani Sarvestani et al. 2018). In other scientific papers, we can also find the author's original solutions describing the research stands designed for this type of test (Majid et al. 2018; McShane et al. 2006; Mohammadabadi et al. 2018). In these solutions, the impactor measures the deflections of the tested samples at the point of impact. An original testing device was designed (Fig. 6) to determine the bottom face sheet's reaction to the impact and assess the influence of the type of core on the panel's deflections. This impact test machine was constructed of square-cross section aluminum profiles. The main structural element is a frame (1) on which a transverse beam with an electromagnetic lock (2) releasing the impactor (3) with a diameter of 25.4 mm is mounted. The impactor is equipped with AXIS FB10k strain gauge (manufactured by AXIS Sp. z o.o. Gdańsk, Poland) with a measurement range of up to 10 kN, measurement accuracy of 2 N and force measurement frequency of up to 1 kHz (4). The total weight W (kg) of the impactor including the strain gauge was 5 kg. At the bottom of the rack (1) there is a handle for installation of non-sliding sample (5). A laser displacement meter optoNCDT 1320 with a measuring range of up to 25 mm, a measuring accuracy of 0.002 mm and a measuring frequency of up to 2 kHz was used.

The samples were placed between two clamping frames ensuring rigid support over the entire perimeter. The sample clamps design also ensured that the location of a

Table 3 Physico-mechanical properties of materials. Standard deviations given in parentheses

Properties	MC (%)	Density (kg/m³)	υ_{yx}	υ_{xy}	E_y (MPa)	E_x	σ_y	σ_x
HPL	-	1412 (56)	0.304 (0.005)	0.313 (0.025)	11,197 (1482)	9719 (636)	72.7 (17.2)	50.8 (13.0)
HDF	5.17 (0.21)	852 (12)	$\upsilon_{yx} = \upsilon_{xy}$ 0.301 (0.082)		$E_x = E_y$ 3961 (370)		$\sigma_x = \sigma_y$ 26.1 (4.0)	
LW	0.69 (0.25)	903 (12)	$\upsilon_{yx} = \upsilon_{xy}$ 0.288 (0.067)		$E_x = E_y$ 831 (15)		$\sigma_x = \sigma_y$ 12.4 (1.3)	
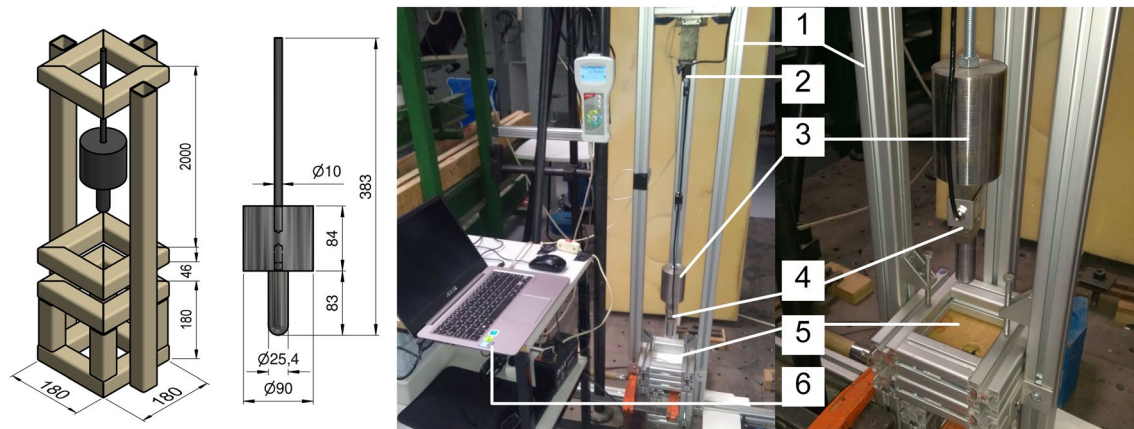
Fig. 6 Device for measuring the force and deflection of samples during low velocity impact: 1 frame, 2 electromagnetic lock, 3 impactor, 4 strain gauge AXIS FB10k series, 5 sample, 6 computer

lattice core of each sample in relation to the impactor was reproducible. The impactor was suspended using the electromagnetic lock so that it would strike the center of the sample during free fall. The height H (mm) of the impactor suspension above the sample's surface was $H_{10} = 100$ mm and $H_{30} = 300$ mm. This layout ensured that the potential energy E_p (J) of the impactor was equal to $E_{p10} = 4.91$ J and $E_{p30} = 14.72$ J, respectively. At the moment, the impactor was released from the electromagnetic lock, the impact force F_d (N), the deflection H_i (mm), and time (ms) of penetration by the impactor in the sample were simultaneously measured with a frequency equal to 2 kHz.

The potential energy of the impactor was calculated from Eq. 1,

$$E_p = MgH, \qquad (1)$$

where: $M = 5$ kg impactor mass, $g = 9.81$ m/s^2 earth acceleration, $H = 100$ mm and 300 mm impactor drop height. Impact energy E_i(J) was calculated based on Eq. 2,

$$E_i = MgH_i. \qquad (2)$$

Impact energy is the energy absorbed by the sample at the moment of an impact. Total energy E_T (J) during an impact of the impactor on the sample was calculated from Eq. (3) using the method of graphical integration of the function $F_d = f(H_i)$ drawn based on the direct test results,

$$E_T = \int_o^{H_i} F_d(H_i) dH_i. \qquad (3)$$

The amount of energy absorbed by the sample was calculated from Eq. 4,

$$K_a = \frac{E_i}{E_T} \times 100\%. \qquad (4)$$

Then, a dynamic impact factor K was calculated,

$$K = \frac{F_d}{F_s}, \qquad (5)$$

where: $F_s = Mg$ the value of the static load.

2.4 Statistical analysis

The results of experimental tests were analyzed statistically using ANOVA with multi-factor classification. First of all, the significance of the influence of the face sheet material type (M), the potential energy of the impactor (E$_p$), and core cell type (TC) on the amount of energy absorbed by the honeycomb sandwich panels was determined. The significance of the interactions: M* E$_p$, M*TC, E$_p$*TC, as well as M*E$_p$*TC was also determined. Differences between the average values of particular groups were also investigated using Tukey's test (HSD). All calculations were performed using the Statistica 13.1 program (StatSoft Polska Sp. z o.o., Kraków, Poland).

3 Results and discussion

3.1 Compressive strength of panels

Figure 7 shows the relationship between load and deflection for the compression tests of sandwich panels. Figure 8 shows
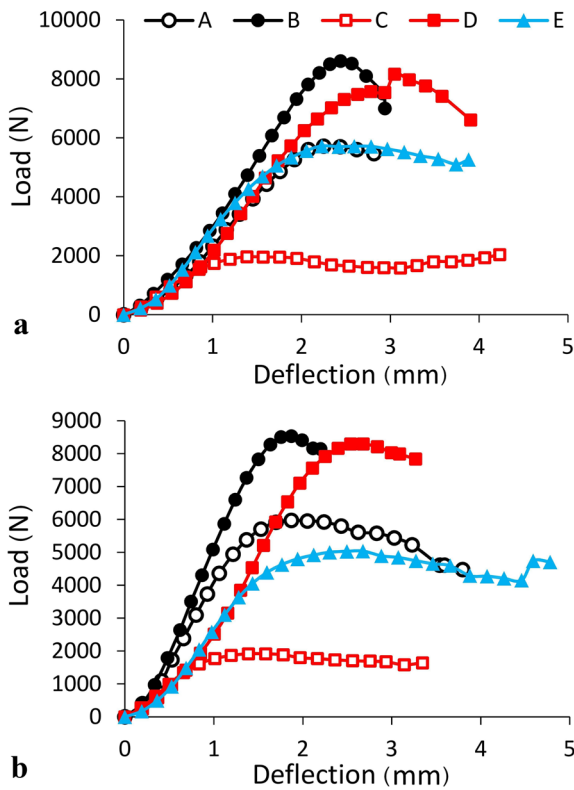
Fig. 7 Dependence of force on deflection in compression test of sandwich panels: **a** with HDF face sheets, **b** with HPL face sheets

pictures of damages to these panels. From the observation of the deflection as a function of force progression (Fig. 7) it follows that during compression of all types of panels with different cores, no sudden cracks nor load drops due to rib fracture occurred. There also were no symptoms of damage in adhesive joints between core and face sheets. The curves are usually smooth, which indicates the dominance of normal (compressive) stresses rather than tangential (shear) stresses in the core elements. Figure 8 also clearly shows that the cell ribs were mainly subjected to bending and compression, while B-type cores were distinguished by small cross-section of the cell ribs and buckling. This figure and graph 7 also illustrate that the core and face sheet bonding were not damaged in any of these cases. The density and compression strength of the tested sandwich panels were compared using Fig. 9.

As shown in Fig. 9, the increase in compressed panels' density did not increase their strength. With a B-type core, the panel, regardless of the type of the face sheet, was characterized by the highest compression resistance (2.61 MPa). In this case, the density of the panel is the lowest among the tested ones. Thus, the high strength of the panel is due to the isotropic structure of the core and the high value of the cell ribs' inclination angle $\varphi_x = \varphi_y = 65°$. For this type of core, cell rib buckling was also observed (Fig. 8), indicating a clear transfer of dominant loads along the rib axis. The lowest compression strength was observed in the case of panels with C-type cores. They were distinguished by the highest density but at the same time by the lowest value of the inclination angle of the cell ribs $\varphi_x = \varphi_y = 26°$. Due to this angle's low value, the cell ribs were mainly bent, which is illustrated in Fig. 8. It was reflected by low compression strength of panels with face sheets produced of HPL and HDF, of 0.59 MPa and 0.6 MPa, respectively. In

Fig. 8 Illustration of core damages in the compression test of sandwich panels: **a** with HDF face sheets, **b** with HPL face sheets
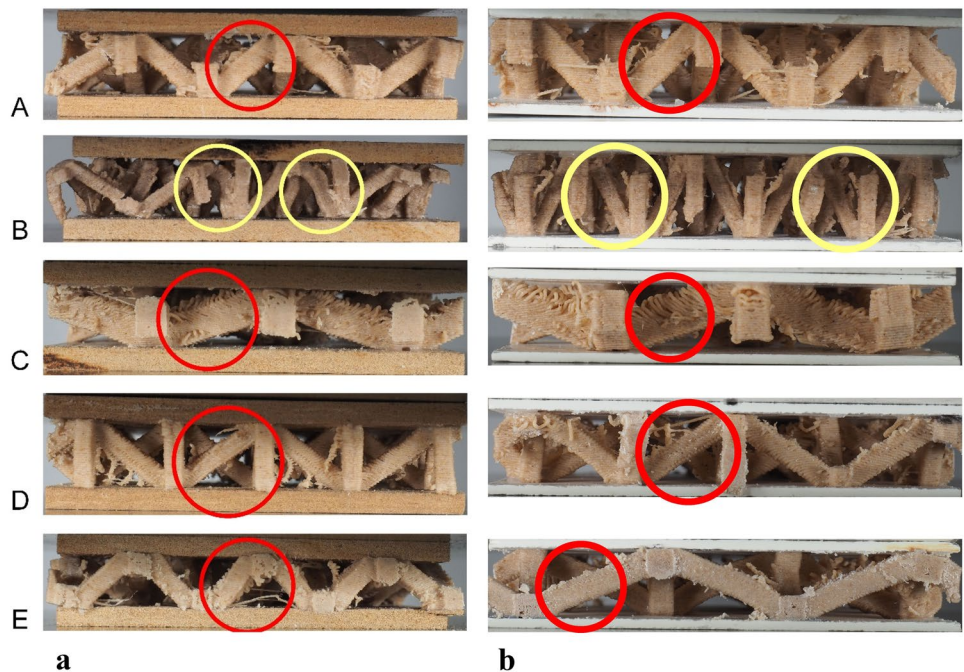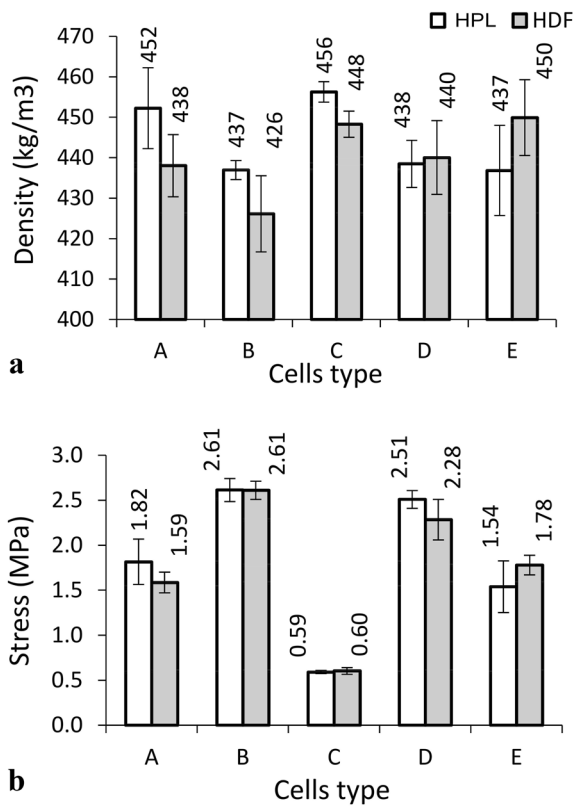
Fig. 9 Density (**a**) and compression strength (**b**) of sandwich panels

core and HDF face sheet, an increase in strength of 15% was observed. Higher compressive strength of panels with HPL face sheet results from the high value of HPL elasticity modulus. Compared to HDF, the HPL modulus is 2.83 times higher (Table 3). This mechanical property of materials results in fewer strains of the face sheets during compression. Other authors also came to similar conclusions. A kind of innovative honeycomb sandwich with ceramic tile was investigated for its bending behavior by Wang et al. (2019). As confirmed, the ceramic tile largely enhances the structure's stiffness, contributing a lot to promoting the bending resistance capacity.

3.2 Influence of panel type on the impact force and the dynamic impact factor

Figure 10 shows the dependence of the impact force on time for the samples with MDF and HPL face sheets for two levels of potential energy $E_{p10} = 4.91$ J and $E_{p30} = 14.72$ J, respectively. Regardless of the sample type, the shape of all curves resembles a sinusoid. The time of impact of HDF and HPL samples with the energy $E_{p10} = 4.91$ J is approximately 30 ms. In the case of an impact with energy $E_{p30} = 14.72$ J of HDF samples, the time amounts to about 25 ms, and for the HPL samples, it is longer by about 5 ms. Figure 10 also shows the maximum forces measured during the impact.

The dynamic impact factor K can better illustrate the nature of this load. This coefficient determines the overload acting upon the sample in relation to the static load ($F_d = 49.05$ N). As shown in Fig. 11a, c, for potential energy $E_{p10} = 4.91$ J, the K-factors of sandwich panels with HDF

most cases, the strength of honeycomb panels with HPL face sheets exceeded the strength of panels with HDF face sheets by 1% to 14%. Only in the case of panels with E-type

Fig. 10 Dependence of the impact force on time: **a**, **b** samples with HDF face sheet, E_p 4.91 J and 14.72 J respectively, **c**, **d** samples with HPL face sheet, E_p 4.91 J and 14.72 J respectively
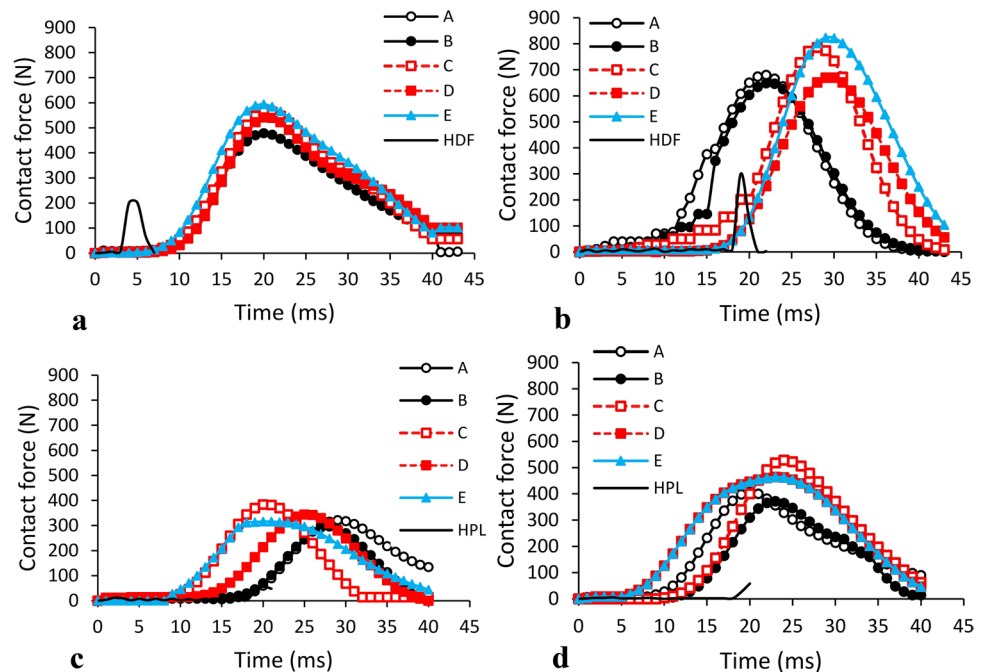
Fig. 11 Dynamic impact factor: **a**, **b** samples with HDF face sheet, E_p 4.91 J and 14.72 J respectively, **c**, **d** samples with HPL face sheet, E_p 4.91 J and 14.72 J respectively
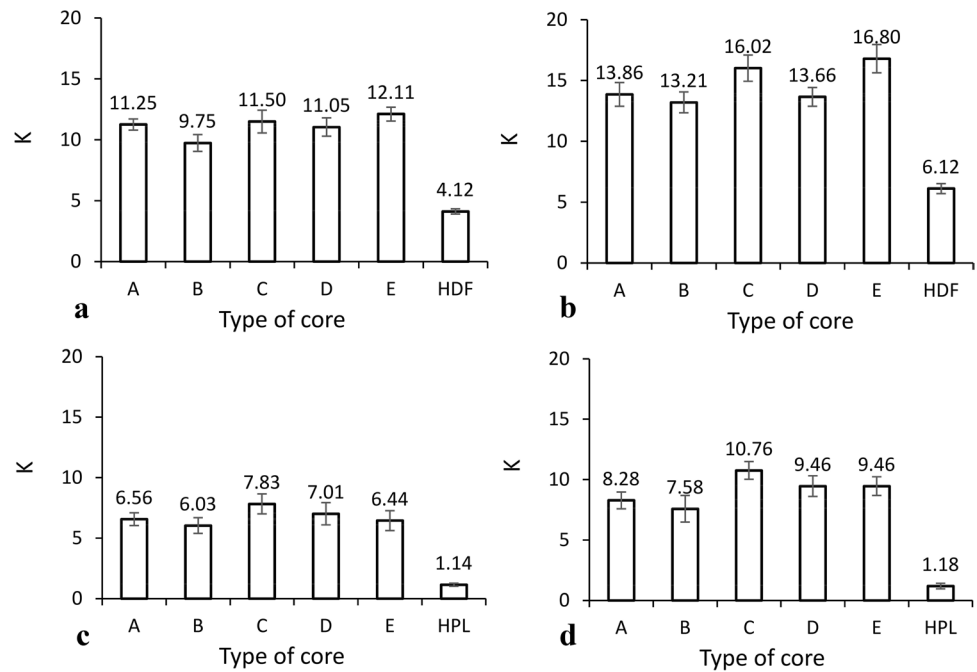
face sheets are 47% to 88% greater than the respective factors characteristic for panels HPL face sheets. Face sheets made of HDF boards have a 2.6 times higher dynamic impact factor in relation to face sheets made of HPL. An increase in the height of free fall of the impactor to 300 mm caused an increase in potential energy $E_{p30} = 14.72$ J. Figure 11b, d shows that in this case, the K-factors for sandwich panels with HDF face sheets are greater by 44% to 76% compared to the respective factors characteristic for panels with HPL face sheets. HDF panels have a higher dynamic impact factor than the face sheets made of HPL. Therefore, it can be assumed that the dynamic load causes a very high overload in face sheets made of HDF, which can damage the sandwich panel surface and core structure. In addition, the effect of the type of core cell on the dynamic impact factor's value is noticeable. The sandwich panels with a B-type core have the lowest coefficient K. In panels with HDF face sheets and E-type core and panels with HPL face sheets and C-type core, K-value was highest.

This regularity is closely related to the density of the tested sandwich panels, which was confirmed in Fig. 9a. In the group of panels with HDF face sheets, panels with E-type core, and in the group of panels with HPL face sheets, panels with C-type core are characterized by the highest density.

Figure 12 illustrates different types of sample damage. Impacts from a height of 100 mm ($E_{p10} = 4.91$ J) cause slight dents in HDF boards, and significant dents in HPL face sheets. In these cases, there were no cracks or bulges in the bottom face sheets. The impacts from a height of 300 mm ($E_{p30} = 14.72$ J), however, cause significant
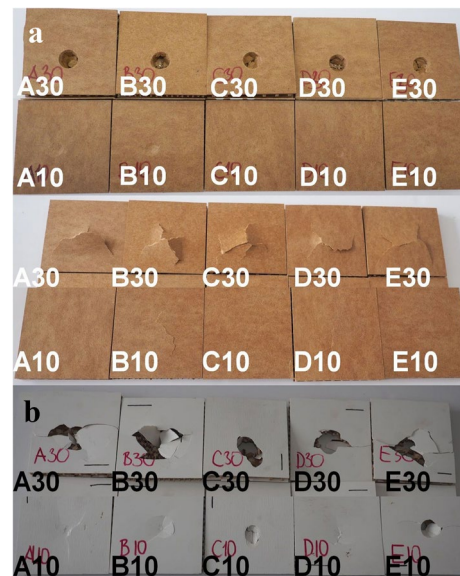
Fig. 12 Images of post-impact damages: **a** HDF face sheet, **b** HPL face sheet. Marks 10 and 30 correspond to $E_{p10} = 4.91$ J and $E_{p30} = 14.72$ J

perforations in the upper HDF face sheet as well as cracks and bulges in the bottom face sheets. For panels with HPL face sheets, extensive cracks in the upper face sheet and almost complete destruction of the bottom face sheets were observed. This is a direct result of the higher stiffness of HPL in relation to the modulus of linear elasticity of HDF (Table 3).

3.3 Influence of face sheet type and height of free fall of an impactor on impact resistance of a sandwich panel

The relationship between total energy E_T (J) and deflection H_i (mm) of the sandwich panel's face sheet is shown in Fig. 13. Using the graphical integration method, the total impact energy was calculated for each of the samples, and the average values are summarized in Table 4. The data present that the total energy amount depends on the impactor's potential energy E_P (J) (free fall height). For panels with HDF face sheet for $E_{p30} = 14.72$ J, the amount of energy during impact is 77% to 126% higher than $E_{p10} = 4.91$ J. The panel with an A-type core represents the most advantageous ratio. A certain anomaly was observed, however, in the case of D-type core panels. In this case, the difference is minimal and perhaps statistically insignificant. For panels with HPL face sheets for $E_{p30} = 14.72$ J, the amount of energy during impact is 161% to 223% higher than $E_{p10} = 4.91$ J. Panels with A-D cores have similar energy gains (from 212 to 223%). Only the panel with E cells is distinguished by a smaller increase in total energy (161%).

Figure 14 illustrates the impact of the energy absorption factor values for samples with HDF and HPL face sheet. Figure 14 shows that for panels with HDF face sheets for $E_{p30} = 14.72$ J, the impact energy absorption factor is 0.4% to 132% higher when compared to $E_{p10} = 4.91$ J. The opposite phenomenon was observed for panels with HPL face sheets. For $E_{p10} = 4.91$ J, the impact energy absorption factor is 26% to 97% higher compared to $E_{p30} = 14.72$ J. The main reason for this regularity is the significant difference in density and

Table 4 Impact force F_d and total energy E_T. Standard deviations given in parentheses

Type of core	E_T (J)			
	HDF		HPL	
	E_{p10}	E_{p30}	E_{p10}	E_{p30}
A	1.50/(0.21)	3.39/(0.72)	1.87/(0.39)	5.88/(1.18)
B	2.78/(0.43)	5.79/(0.93)	1.06/(0.22)	3.33/(0.86)
C	2.39/(0.46)	4.23/(0.96)	1.54/(0.39)	4.93/(1.01)
D	2.68/(0.52)	2.56/(0.64)	1.85/(0.41)	5.97/(1.21)
E	2.06/(0.41)	4.02/(0.87)	2.29/(0.53)	5.97/(1.03)
Face	0.44/(0.08)	1.21/(0.02)	0.24/(0.05)	0.46/(0.09)

linear elasticity modulus of HDF and HPL. As shown in Table 3, linear elasticity modulus and density of HPL are higher than of HDF panels by 183% and 66%, respectively.

3.4 Influence of core cell type and height of free fall of an impactor on impact resistance of a sandwich panel

Based on Fig. 13 and Table 4, we can also observe how the total energy changes depending on the type of cells forming the sandwich panel's core. In the case of panels with HDF face sheets, for $E_{p10} = 4.91$ J, the highest total energy ($E_T = 2.78$ J) is represented by samples with B-type core, followed by cells D, C, E, and A, respectively. For the height of fall of 300 mm ($E_{p30} = 14.72$ J), the highest total energy ($E_T = 5.79$ J) is also represented by samples with B-type core, followed by cells C, E, A, and D,

Fig. 13 Dependence of E_a (J) on H_i (mm): **a, b** samples with HDF face sheet, E_p 4.91 J and 14.72 J respectively, **c, d** samples with HPL face sheet, E_p 4.91 J and E_p 14.72 J respectively
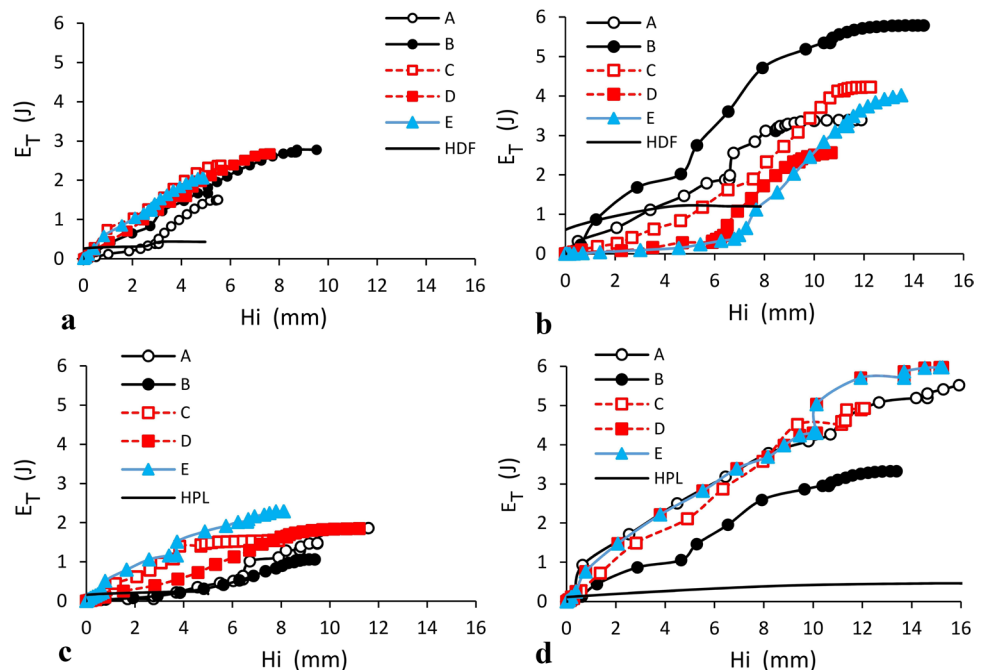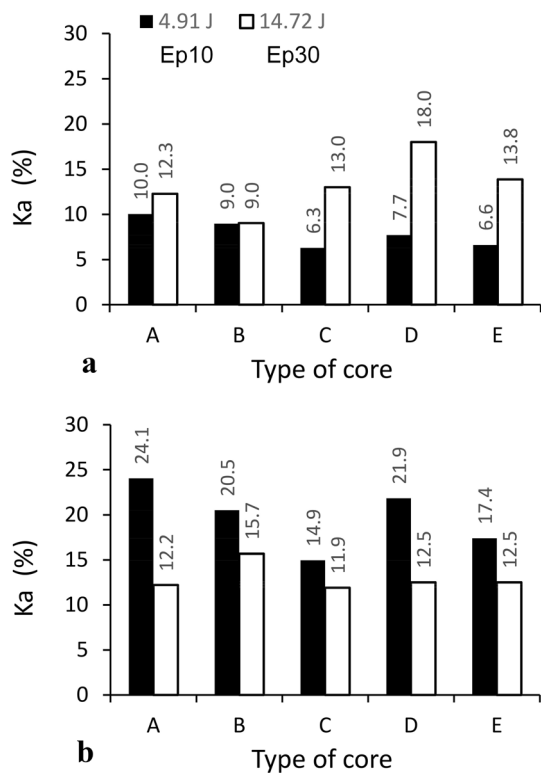
Fig. 14 Impact energy absorption factor: **a** samples with HDF face sheet, **b** samples with HPL face sheet

Table 5 Variance analysis results sheet

	SS	DF	MS	F	p
Mark	18,136 .42	1	18,136 .42	7522 .477	0 .000000
M	835 .18	1	835 .18	346 .410	0 .000000
H	13 .61	1	13 .61	5 .646	0 .019885
TC	165 .32	4	41 .33	17 .142	0 .000000
M*H	912 .13	1	912 .13	378 .327	0 .000000
M*TC	98 .27	4	24 .57	10 .190	0 .000001
H*TC	154 .43	4	38 .61	16 .013	0 .000000
M*H*TC	147 .72	4	36 .93	15 .318	0 .000000
Error	192 .88	80	2 .41		

SS sum of squares, *DF* degrees of freedom, *MS* mean sum of squares, *F* test value, *p* probability

respectively. In the case of panels with HPL face sheets for E_{p10} = 4.91 J, the highest total energy (E_T = 2.29 J) is represented by samples with E-type core, followed by A, D, C, and B cells. For the height of fall of 30 cm (E_{p30} = 14.72 J), the highest total energy (E_T = 5.97 J) is obtained from samples with core types D and E, followed by cells A, C, and B, respectively.

Figure 14 shows that in the case of panels made with HDF face sheets and subjected to impact from a height of 10 cm, the impact energy absorption factor has the highest value for A-type core (10%), followed by B (9%), D (7.7%), E (6.6%) and C (6.3%). This order changes when the samples are subjected to impact from a height of 30 cm. In the latter case, the highest value of the impact energy absorption factor is shown by the samples with the following types of core: D (18%), E (13.8%), C (13%), A (12.3%), and B (9%). A change in the sandwich panel's face sheet also changes the effect of the type of individual cores on the value of the impact energy absorption factor. In the case of panels made with HPL face sheet and subjected to impact from a height of 10 cm, the impact energy absorption factor has the highest value for A-type core (24.1%), followed by D (21.9%), B (20.5%), E (17.4%) and C (14.9%). When the samples are subjected to an impact from a height of 30 cm, the highest value of the impact energy absorption factor is shown by the

samples with the following types of core: B (15.7%), D and E (12.5%), A (12.2%), and C (11.9%).

A detailed statistical analysis of the influence of individual factors on the value of the impact energy absorption factor is presented below.

4 Results of statistical analysis

Table 5 presents the variance of the influence of particular variables and their interactions on the value of the impact energy absorption factor. This table shows that the impact of all variables is statistically significant. The graphical interpretation of the interaction effect is presented in Fig. 15.

For all core types, the potential energy E_p (J) of the free fall of the impactor from 100 and 300 mm has a significant influence on the increase in the impact energy absorption factor. For panels with HPL face sheets and all types of cores, E_p (J) has a significant influence on reducing the value of the impact energy absorption factor. Furthermore, the highest increases or decreases in the value of K_a (%) occur in the case of D-type cells and the lowest in B-type cells. As shown in Fig. 9, B-type core panels have the lowest density and the highest compression strength. It results directly from the cell geometry, especially the largest angle of inclination of the arms. Figure 11 shows that B-type panels have the lowest values of the dynamic impact factor. These observations conclude that B cell favorably minimizes the differences in absorbed energy when using different face sheets and the different energy values during the low-velocity impact. Considering the amount of absorbed energy, the most attractive is the panel with the D-type core. For samples with HDF face sheet, the amount of energy absorbed increases significantly with the increase in the impactor's potential energy. Simultaneously, the amount of energy absorbed is drastically reduced when HPL face sheet is used. Although panels with a D-type core have a similar

Fig. 15 Graphical interpretation of the interaction effect

density to those with a B-type core, they have significantly higher values of the dynamic impact factor (Fig. 9 and 11). This regularity is influenced by their geometry, especially the cells' arms' width and the different angles of their inclination. Therefore, the observation can be made that this is the cell with the most favorable properties for absorbing low velocity impact energy.

Table 6 summarizes Tukey's test (HSD) results. In this table, only the links indicating the lack of significance of differences between variables were marked. In other cases, the differences proved to be statistically significant, which ultimately allowed the selection of D and B cells as the most

advantageous in terms of energy absorption capacity during low velocity free fall.

5 Conclusion

Based on the analysis of the obtained test results, the following conclusions and observations were formulated:

1. The highest compression strength characterized the panel with B-type core. This panel is distinguished by the lowest density and isotropic properties of the core with a high angle of inclination of the cell ribs $\varphi_x = \varphi_y = 65°$.
2. The lowest compression strength was observed in the case of the panel with a C-type core. It has the highest density but at the same time the lowest value of the angle of inclination of the cell ribs $\varphi_x = \varphi_y = 26°$.
3. Sandwich panels with a B-type core have the lowest value of the dynamic impact factor. The highest values are found in panels with HDF face sheets and E-type core, whereas in the group of panels with HPL face sheets, the C-type cores. This regularity is closely related to the density of the sandwich panels.
4. The dynamic load causes a very high overload in face sheets made of HDF, which results in damage to the sandwich panel surface and core structure.
5. Cells of type B favorably minimize the differences in absorbed energy when using different face sheets and different energy values of low velocity impact.

Table 6 List of variables for which no significant impact was demonstrated

M			HDF	HDF	HDF	HDF	HDF	HDF	HDF	HDF	HDF	HDF	HPL	HPL	HPL	HPL	HPL	HPL
	E_p		10	10	10	10	10	30	30	30	30	30	10	10	10	30	30	30
		TC	A	B	C	D	E	A	B	C	D	E	A	B	C	A	B	C
HDF	10	D	x	x	x													
HDF	10	E	x	x	x	x												
HDF	30	A	x	x														
HDF	30	B	x	x	x	x	x	x										
HDF	30	C	x					x										
HDF	30	E						x		x								
HPL	10	B									x		x					
HPL	10	C						x		x	x	x						
HPL	10	D											x	x				
HPL	10	E									x	x			x	x		
HPL	30	A	x	x				x	x	x		x				x		
HPL	30	B						x		x	x	x				x	x	
HPL	30	C	x	x				x	x	x		x				x	x	
HPL	30	D	x	x				x	x	x		x			x	x	x	x
HPL	30	E	x	x				x	x	x		x			x	x	x	x

6. Considering the amount of absorbed energy, the most attractive is the panel with the D-type core. For samples with HDF face sheet, the amount of energy absorbed increases significantly with the increase in the impactor's potential energy. Simultaneously, the amount of energy absorbed is drastically reduced when HPL face sheet is used.

Compliance with ethical standards

Conflict of interest The authors declare that they have no conflict of interest.

References

Almgren R (1985) An isotropic three-dimensional structure with Poisson's ratio =−1. J Elast 15:427–430. https://doi.org/10.1007/BF00042531

Barboutis I, Vassiliou V (2005) Strength properties of lightweight paper honeycomb panels for the furniture. In: 10th International Scientific Conference of Engineering Design (Interior and Furniture Design), pp 17–18

Bogoeva-Gaceva G, Avella M, Malinconico M et al (2007) Natural fiber eco-composites. Polym Compos 28:98–107. https://doi.org/10.1002/pc.20270

Boonkong T, Shen YO, Guan ZW, Cantwell WJ (2016) The low velocity impact response of curvilinear-core sandwich structures. Int J Impact Eng 93:28–38. https://doi.org/10.1016/j.ijimpeng.2016.01.012

Chen Y, Hou S, Fu K et al (2017) Low-velocity impact response of composite sandwich structures: modelling and experiment. Compos Struct 168:322–334. https://doi.org/10.1016/j.compstruct.2017.02.064

Evans KE (1991) Auxetic polymers: a new range of materials. Endeavour 15:170–174. https://doi.org/10.1016/0160-9327(91)90123-S

Gao Q, Ge C, Zhuang W et al (2019) Crashworthiness analysis of double-arrowed auxetic structure under axial impact loading. Mater Des 161:22–34. https://doi.org/10.1016/j.matdes.2018.11.013

Guj L, Sestieri A (2007) Dynamic modeling of honeycomb sandwich panel. Arch Appl Mech 77:779–793. https://doi.org/10.1007/s00419-007-0121-5

Han B, Zhang Z-J, Zhang Q-C et al (2017) Recent advances in hybrid lattice-cored sandwiches for enhanced multifunctional performance. Extrem Mech Lett 10:58–69. https://doi.org/10.1016/j.eml.2016.11.009

He W, Liu J, Wang S, Xie D (2018) Low-velocity impact response and post-impact flexural behaviour of composite sandwich structures with corrugated cores. Compos Struct 189:37–53. https://doi.org/10.1016/j.compstruct.2018.01.024

Holbery J, Houston D (2006) Natural-fiber-reinforced polymer composites in automotive applications. JOM 58:80–86. https://doi.org/10.1007/s11837-006-0234-2

Jin M, Hu Y, Wang B (2015) Compressive and bending behaviours of wood-based two-dimensional lattice truss core sandwich structures. Compos Struct 124:337–344. https://doi.org/10.1016/j.compstruct.2015.01.033

Jin X, Wang Z, Ning J et al (2016) Dynamic response of sandwich structures with graded auxetic honeycomb cores under blast loading. Compos Part B Eng 106:206–217. https://doi.org/10.1016/j.compositesb.2016.09.037

Kao Y-T, Amin AR, Payne N et al (2018) Low-velocity impact response of 3D-printed lattice structure with foam reinforcement. Compos Struct 192:93–100. https://doi.org/10.1016/j.compstruct.2018.02.042

Kavermann SW, Bhattacharyya D (2019) Experimental investigation of the static behaviour of a corrugated plywood sandwich core. Compos Struct 207:836–844. https://doi.org/10.1016/j.compstruct.2018.09.094

Kılıçaslan C, Güden M, Odaci IK, Taşdemirci A (2013) The impact responses and the finite element modeling of layered trapezoidal corrugated aluminum core and aluminum sheet interlayer sandwich structures. Mater Des 46:121–133. https://doi.org/10.1016/j.matdes.2012.09.059

Klimek P, Wimmer R, Brabec M, Sebera V (2016) Novel sandwich panel with interlocking plywood kagome lattice core and grooved particleboard facings. BioResources 11:195–208. https://doi.org/10.15376/biores.11.1.195-208

Kolpakov AG (1985) Determination of the average characteristics of elastic frameworks. J Appl Math Mech 49:739–745. https://doi.org/10.1016/0021-8928(85)90011-5

Lakes RS (1987) Foam structures with a negative Poisson's ratio. Science (80-) 235:1038–1040. https://doi.org/10.1126/science.235.4792.1038

Lakes RS (2017) Negative-Poisson's-ratio materials: Auxetic solids. Annu Rev Mater Res 47:63–81. https://doi.org/10.1146/annurev-matsci-070616-124118

Li T, Wang L (2017) Bending behavior of sandwich composite structures with tunable 3D-printed core materials. Compos Struct 175:46–57. https://doi.org/10.1016/j.compstruct.2017.05.001

Lim T-C (2017) Analogies across auxetic models based on deformation mechanism. Phys status solidi – Rapid Res Lett 11:1600440. https://doi.org/10.1002/pssr.201600440

Lim T-C (2015) Auxetic materials and structures. Springer Singapore, Singapore

Liu Y, Zhou C, Cen B, Zeng Z, Lu X, Zhu X (2017) Compression property of a novel lattice sandwich structure. Compos B 117:130–137. https://doi.org/10.1016/j.compositesb.2017.02.036

Majid DL, Mohd Jamal Q, Manan NH (2018) Low-velocity impact performance of glass fiber, kenaf fiber, and hybrid glass/kenaf fiber reinforced epoxy composite laminates. BioResources 11:8839–8852. https://doi.org/10.15376/biores.13.4.8839-8842

Maslej M, Smardzewski J (2019) Experimental testing of elastic properties of LayWood pyramidal cores. BioResources 14:9686–9703. https://doi.org/10.15376/biores.14.4.9686-9703

McShane GJ, Radford DD, Deshpande VS, Fleck NA (2006) The response of clamped sandwich plates with lattice cores subjected to shock loading. Eur J Mech A/Solids 25:215–229. https://doi.org/10.1016/j.euromechsol.2005.08.001

Menna C, Zinno A, Asprone D, Prota A (2013) Numerical assessment of the impact behavior of honeycomb sandwich structures. Compos Struct 106:326–339. https://doi.org/10.1016/j.compstruct.2013.06.010

Mines RAWW, Tsopanos S, Shen Y et al (2013) Drop weight impact behaviour of sandwich panels with metallic micro lattice cores. Int J Impact Eng 60:120–132. https://doi.org/10.1016/j.ijimpeng.2013.04.007

Mohammadabadi M, Yadama V, Yao L, Bhattacharyya D (2018) Low-velocity impact response of wood-strand sandwich panels and their components. Holzforschung 681:689

Mohanty AK, Misra M, Drzal LT (2002) Sustainable bio-composites from renewable resources: opportunities and challenges in the green materials world. J Polym Environ 10:19–26. https://doi.org/10.1023/A:1021013921916

Qi G, Ma L (2018) Experimental investigation of composite pyramidal truss core sandwich panels with lightweight inserts. Compos Struct 187:336–343. https://doi.org/10.1016/j.compstruct.2017.12.071

Sam-Brew S, Semple K, Smith GD (2011) Preliminary experiments on the manufacture of hollow core composite panels. For Prod J 61:381–389. https://doi.org/10.13073/0015-7473-61.5.381

Schwingshackl CW, Aglietti GS, Cunningham PR (2006) Determination of honeycomb material properties: Existing theories and an alternative dynamic approach. J Aerosp Eng 19:177–183. https://doi.org/10.1061/(ASCE)0893-1321(2006)19:3(177)

Smardzewski J, Jasińska D (2016) Mathematical models and experimental data for HDF based sandwich panels with dual corrugated lightweight core. Holzforschung 71:265–273. https://doi.org/10.1515/hf-2016-0146

Smardzewski J, Wojciechowski KW, Poźniak A (2018) Auxetic lattice truss cores fabricated of LayWood. BioResources 13:8823–8838. https://doi.org/10.15376/biores.13.4.8823-8838

Smardzewski J, Wojciechowski KW (2019) Response of wood-based sandwich beams with three-dimensional lattice core. Compos Struct 216:340–349. https://doi.org/10.1016/j.compstruct.2019.03.009

Spadoni A, Ruzzene M, Scarpa F (2005) Chiral hexagonal cellular sandwich structures: dynamic response. Proc SPIE 5764:324–334. https://doi.org/10.1117/12.600021

Sun G, Chen D, Huo X et al (2018) Experimental and numerical studies on indentation and perforation characteristics of honeycomb sandwich panels. Compos Struct 184:110–124. https://doi.org/10.1016/j.compstruct.2017.09.025

Wang Z (2019) Recent advances in novel metallic honeycomb structure. Compos Part B Eng 166:731–741. https://doi.org/10.1016/j.compositesb.2019.02.011

Wang Z, Li Z, Xiong W (2019) Experimental investigation on bending behavior of honeycomb sandwich panel with ceramic tile facesheet. Compos Part B Eng 164:280–286. https://doi.org/10.1016/j.compositesb.2018.10.077

Wojciechowski KW (1989) Two-dimensional isotropic system with a negative Poisson ratio. Physiics Lett A 137:60–64. https://doi.org/10.1016/0375-9601(89)90971-7

Wojciechowski KW (1987) Constant thermodynamic tension Monte Carlo studies of elastic properties of a two-dimensional system of hard cyclic hexamers. Mol Phys 61:1247–1258. https://doi.org/10.1080/00268978700101761

Wojciechowski KW, Alderson A, Grima JN, Scarpa F (2020) Auxetics and other systems with "negative" characteristics. Phys status solidi 257:2000496. https://doi.org/10.1002/pssb.202000496

Xiong J, Ghosh R, Ma L et al (2014a) Bending behavior of lightweight sandwich-walled shells with pyramidal truss cores. Compos Struct 116:793–804. https://doi.org/10.1016/j.compstruct.2014.06.006

Xiong J, Ma L, Stocchi A et al (2014b) Bending response of carbon fiber composite sandwich beams with three dimensional honeycomb cores. Compos Struct 108:234–242. https://doi.org/10.1016/j.compstruct.2013.09.035

Xu G, dong, Yang F, Zeng T, et al (2016) Bending behavior of graded corrugated truss core composite sandwich beams. Compos Struct 138:342–351. https://doi.org/10.1016/j.compstruct.2015.11.057

Xu GD, Zhai JJ, Zeng T et al (2015) Response of composite sandwich beams with graded lattice core. Compos Struct 119:666–676. https://doi.org/10.1016/j.compstruct.2014.09.042

Xue Z, Hutchinson JW (2006) Crush dynamics of square honeycomb sandwich cores. Int J Numer Methods Eng 65:2221–2245. https://doi.org/10.1002/nme.1535

Yazdani Sarvestani H, Akbarzadeh AH, Mirbolghasemi A, Hermenean K (2018) 3D printed meta-sandwich structures: Failure mechanism, energy absorption and multi-hit capability. Mater Des 160:179–193. https://doi.org/10.1016/j.matdes.2018.08.061

Yu X, Zhou J, Liang H et al (2018) Mechanical metamaterials associated with stiffness, rigidity and compressibility: A brief review. Prog Mater Sci 94:114–173. https://doi.org/10.1016/j.pmatsci.2017.12.003

Zhang Q, Yang X, Li P et al (2015) Bioinspired engineering of honeycomb structure—using nature to inspire human innovation. Prog Mater Sci 74:332–400. https://doi.org/10.1016/j.pmatsci.2015.05.001